Research Paper

The Effect of Cold Eddy on Acoustic Propagation (Case Study: Eddy in the Persian Gulf)

Omid MAHPEYKAR[(1)], Amir ASHTARI LARKI[(1)*], Mohammad AKBARI NASAB[(2)]

[(1)] *Department of Physical Oceanography, Faculty of Marine Science and Oceanography*
Khorramshahr University of Marine Science and Technology
Khorramshahr, Iran

[(2)] *Department of Marine Physics, Faculty of Marine and Oceanic Sciences*
University of Mazandaran
Babolsar, Iran

*Corresponding Author e-mail: Ashtari@kmsu.ac.ir

(*received May 21, 2021; accepted April 11, 2022*)

It is essential for oceanographers to study the effects of marine phenomena such as currents, surface mixed layer, eddies, internal waves, and other ocean features on acoustic propagation, as most marine measurement equipment operates on this basis, like sonar. The eddy impact on acoustic transmission in the marine environment is very significant because changes in temperature and salinity disrupt the sound speed due to the presence of eddy, thus the acoustic propagation in the sea. Although cold eddies are in the Persian Gulf widely, one eddy is selected to study their impacts on acoustic propagation because they have similar properties in terms of temperature and salinity. In this research, after identifying eddies in the Persian Gulf automatically, the effect of a cold eddy on acoustic propagation was investigated at different depths using the BELLHOP model. Most eddies are cyclonic with 5–10 km of radius based on algorithm outputs. Studies on the lifespan of eddies showed that the occurrence of cyclonic eddies with a lifespan of more than three days is more than anticyclonic ones. Examination of the eddy effect on acoustic propagation showed that the transmission loss (TL) during the progress of the acoustic wave across the eddy increases with increasing the depth of the sound source. Also, the presence of cold eddy compared to the conditions it does not exist increases the transmission loss. The study of three-dimensional acoustic propagation also confirmed the obtained results in two-dimensional mode and clearly showed the role of cold eddy in increasing the TL.

Keywords: Persian Gulf; cold eddy; transmission loss (TL); acoustic propagation; BELLHOP model.

1. Introduction

Eddy is a rotating current seen in all seas and oceans. These currents have a diameter between 10–500 km, and depending on the basin, their depth can reach up to 1000 meters. Mesoscale eddies have a lifespan of several days to several months and a mean propagation distance a few hundreds of kilometers (Chelton *et al.*, 2011; Zhang *et al.*, 2014; Chang *et al.*, 2015). Also, the direction of rotation of eddies can be counterclockwise or clockwise, which are referred to as cyclones and anticyclones, respectively; and their rotational speed is on average 0.1–0.2 ms^{-1}, but the speed can sometimes reach up to 0.4 ms^{-1} (Chang *et al.*, 2017). Eddies play an important role in various physical and chemical processes (Volkov *et al.*, 2008). The biochemical effects of eddies and their potential relationships with marine organisms have been debated for decades. One of the important effects of eddies is the change in the acoustic propagation in the seas. Because eddies reorder the temperature and salinity field in the oceans, they change the sound speed in the environment and ultimately disrupt the acoustic propagation. These changes cause

the acoustic pressure to be varied non-uniformly as it passes through the eddy, forming a Sound Fixing and Ranging (SoFAR) Channel at some points.

Acoustic propagation patterns and TL variables are very sensitive to the inhomogeneity of temperature and salinity in shallow water (Katsnelson *et al.*, 2012). Structures such as eddies, fronts, thermoclines, internal waves, and the like cause significant temperature and salinity changes in the acoustic propagation environment due to dynamic properties in shallow water. There is ample evidence that these structures can alter acoustic propagation to various degrees (Lysanov *et al.*, 1989; Heathershaw *et al.*, 1990; Lynch *et al.*, 2003; Xu *et al.*, 2009; Lermusiaux *et al.*, 2010). They occur at different spatial and temporal scales, and considerable effects have on acoustic propagation, especially in shallow water. Knowledge about the acoustic propagation mechanism is of particular interest under various climates and weather in the shallow seas since commercial and civilian activities in coastal waters have been increasing rapidly. Fluctuations in acoustic pressure levels resulting from oceanic parameters variations can be transferred into noise fields, leading to different noise patterns in time and space. In this study, the effects of a cold eddy on acoustic propagation in the Persian Gulf as shallow water were investigated.

The general circulation pattern in the Persian Gulf is primarily influenced by the prevailing northwesterly winds and the corresponding momentum and buoyancy fluxes, then by thermohaline forcing and eventually by the tides (Thoppil, Hogan, 2010). The details of the circulation are more complex than a cyclonic gyre due to seasonal changes in water exchange in the Strait of Hormuz, river inflows, wind intensity, and topographic anomalies (Pous *et al.*, 2015). This circulation consists of two scales:

1) Basin-scale is the general circulation and entails two currents: one to the northwest of the Strait of Hormuz along the Iranian coast in the northern part of the basin, the other to Southeast in the southern part of the basin (Reynolds, 1993).
2) Mesoscale involves eddies with various dimensions that happen due to instability and the decomposition of the main rotation into a set of eddies (Fig. 1).

In summer, by reinforcing the stability of the water column and forming strong stratification, eddies form even with a diameter of more than 100 km. In late summer, these eddies alter the overall structure of the Persian Gulf to mesoscale ones. These conditions remain in the basin for two to three months (Thoppil, Hogan, 2010).

Oceanographers and acousticians need to recognize the factors affecting acoustic waves because these waves are widely applied in acoustical oceanography, submarine communications, and the revelation of navigational information. A broad range of specialists have

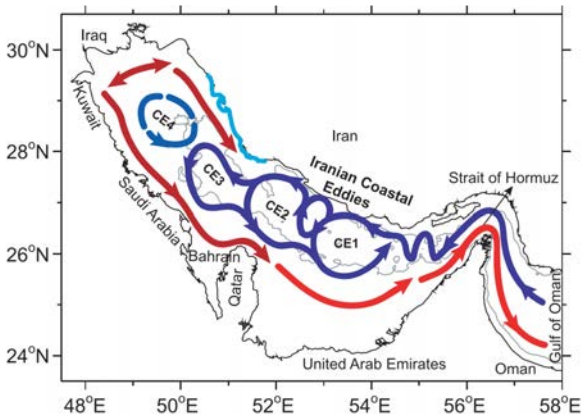

Fig. 1. Mesoscale eddies in the Persian Gulf, CE1, CE2, CE3, and CE4 correspond to the Iranian coastal eddies (Thoppil, Hogan, 2010).

used the methods of underwater acoustics in communication systems, shipping noise, and radiated noise of a typical fishing boat in shallow water (Kochańska *et al.*, 2020; Peng *et al.*, 2018; 2021). Measures such as depth measurement and depth mapping, voice communication, and installation of acoustic arrays to identify subsurface targets are required to have a correct understanding of how acoustic waves propagate in the sea environment.

A few studies have been conducted about the effects of eddies on acoustic propagation in shallow water. The nature of acoustic propagation is generally different in shallow water and deep water (Liang *et al.*, 2014), and study has not been undertaken on this issue so far, especially in the Persian Gulf. Li *et al.* (2012) modeled the mesoscale eddy and its application in the underwater acoustic propagation. For this purpose, a theoretical computational model of ocean mesoscale eddy was developed based on hydrographic measurement data in the sea area of the ocean. The Monterey-Miami Parabolic Equation (MMPE) acoustic model was used to simulate the underwater acoustic propagation under the influence of different types, different intensities and positions of eddies, and different frequencies and depths of sources. The results showed that the warm-core eddy could make the convergence zone "move back" and the width of it increases, while the cold-core eddy can make the convergence zone "move forward" and the width of it decreases. Xiao *et al.* (2019) investigated the effect of the warm eddy on acoustic propagation in the Gulf of Mexico. First, the physical parameters of eddies, such as their lifetime, radius, and spatial distribution, were investigated using an automated method, and a strong warm eddy isolated from the Mexican stream was selected. Then, the effect of this strong warm eddy on acoustic propagation during its lifetime was extensively analyzed by the parabolic equation and explained using normal mode and ray theory. The results showed that warm eddy

could change the propagation path and cause the convergence region to be broader and closer to the acoustic source. In addition, a warm eddy can dissipate acoustic energy, causing deeply integrated energy to tend to a lower normal mode. Chen *et al.* (2019) investigated the two-dimensional structure of a cold eddy in Taiwan and its effect on acoustic propagation. Their results showed that the eddy structure follows that of an ellipsoid, where the most significant anomaly occurs near the center at almost 400 m depth. The horizontal diameter of eddy was 200 km, and its vertical diameter was 500 m. The 2-D sound speed profile feature model for the cold eddy based on the Argo profiles was created by the Empirical Orthogonal Function (EOF) method. With the particular model, the acoustic propagation through both a stationary eddy and a moving eddy was investigated. Results suggest that the presence of the cold eddy could push the convergence zone up to 4 km closer to the source, where it acts as a convex mirror to focus the energy.

2. Materials and methods

In this study, the developed algorithm by Nencioli *et al.* (2010) was used based on the rotation of horizontal velocity components (Vector Geometry Algorithm), using MATLAB software to detect eddies. In terms of appearance, an eddy is defined where the horizontal velocity vector field revolves around a central point. Based on this characteristic, the algorithm uses four constraints to identify eddies. If these four constraints are met, the existence of an eddy is settled and recorded. These four constraints are as follows:

1) Along the west-east section, v component has to reverse in sign across the eddy center and its magnitude has to rise away from it.
2) Along the south-north section, u component has to reverse in sign across the eddy centre and its magnitude has to rise away from it, the rotation rate must be the same as for v.
3) The minimum velocity in the investigation area is considered an eddy centre.
4) The velocity vector directions should rotate with a constant sense revolving around the eddy centre.

The discussed constraints require two parameters to be defined: one for the first, second, and fourth constraints and the other for the third one. The first parameter (A) defines how many grid points away the increases in magnitude of v along the east-west axes and u along the north-south axes are checked. The second parameter (B) defines the dimension (in grid points) of the area used to define the local minimum of velocity. These two parameters determine the accuracy of the algorithm and make the algorithm usable for data of any resolution. On the other hand, depending on the characteristics and spatial resolution of the data set, the values of these parameters required to be precisely adjusted to optimize the performance of the algorithm (Nencioli *et al.*, 2010).

The velocity vector field maps are selected for seven days randomly to validate the algorithm, and experts extract eddies of maps visually. Algorithm efficiency is gained according to a study by Chaigneau *et al.* (2008) by two parameters: the success of detection rate (SDR) and the excess of detection rate (EDR). These parameters are defined as follows:

$$\mathrm{SDR} = \frac{N_c}{N_{te}} \cdot 100, \qquad \mathrm{EDR} = \frac{N_{oa}}{N_{te}} \cdot 100, \tag{1}$$

where N_{te} is the number of real eddies for a data set, detected by the experts, N_c is the number of eddies for the same data set, detected by the experts and registered by the algorithm, and N_{oa} is the number of eddies detected by the algorithm but not recognized as eddies by the experts. In general, SDR and EDR show the detection precision and error in the algorithm, respectively. The larger SDR and smaller EDR lead to better performance of the algorithm.

The velocity components obtained numerical model in the Persian Gulf were selected in seven random days to optimize the algorithm, then SDR and EDR were computed for each different combination of A and B. The algorithm was checked for different values of the two parameters: A varying from 2 to 10 and B varying from 1 to 10, a total of 90 various combinations of A and B were considered to optimize the algorithm. The SDR and EDR diagrams for the various combinations of A and B are given in Fig. 2. Consequently, the combination $A = 3$ and $B = 2$ had the highest accuracy of 85% and the smallest error of 12% for SDR and EDR, respectively.

The acoustic propagation in the sea depends on the sound speed that is a function of temperature, salinity, and ambient pressure. When the sea surface temperature rises in the warm seasons or the hottest part of the day, the sound speed increases near the surface. The sea surface acts as a perfect reflector when it is not wavy, but it disperses acoustic rays in turbulent conditions. We used the Mackenzie formula for sound speed with a standard error of 0.07 m/s as follows (Mackenzie, 1981):

$$\begin{aligned} c = {} & 1448.96 + 4.591T - 5.304 \cdot 10^{-2}T^2 + 2.374 \cdot 10^{-4}T^3 \\ & + 1.340(S-35) + 1.630 \cdot 10^{-2}z + 1.675 \cdot 10^{-7}z^2 \\ & - 1.025 \cdot 10^{-2}T(S-35) - 7.139 \cdot 10^{-13}Tz^3, \end{aligned} \tag{2}$$

where c is sound speed in [ms^{-1}]; z is depth [m]; S is salinity in part per thousand [ppt] in the range from 30 to 40; T is temperature [°C] in the range from 0 to 30.

Ray theory is an alternative theoretical approach to solving the wave equation. The main tenets of ray theory are the existence of a wavefront along which

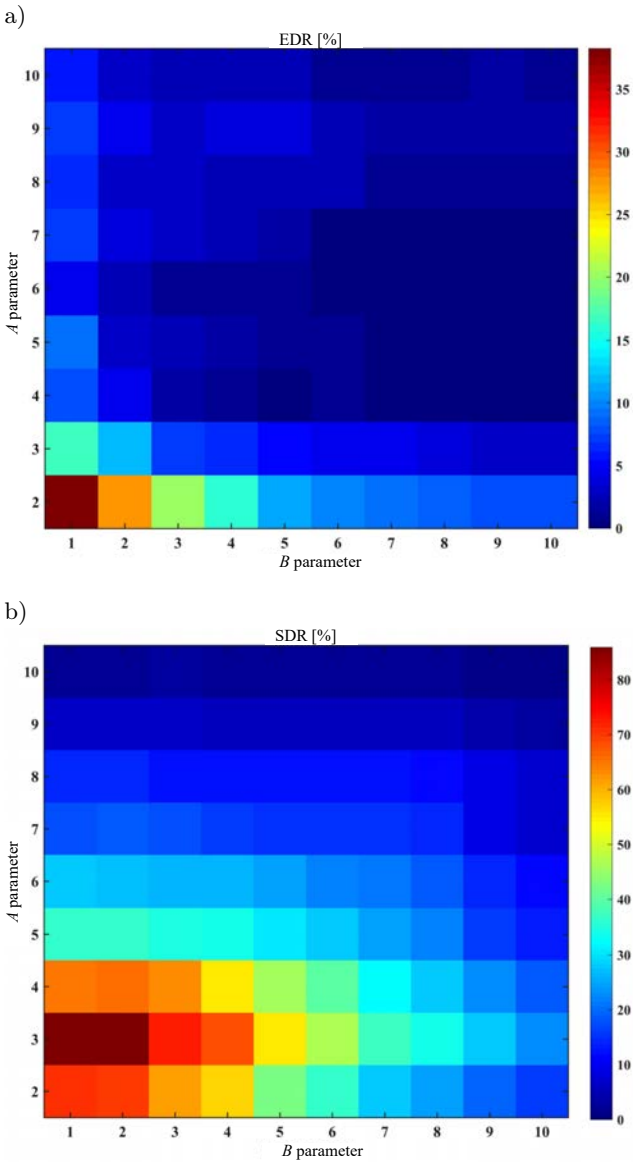

Fig. 2. Different combinations of A and B to optimize the algorithm EDR (a), SDR (b).

the phase of the solution is constant and the existence of rays that describe the spatial location of acoustical energy radiating from the source in a manner analogous to optical ray theory. Ray-tracing programs are commonly used in underwater acoustics to model high-frequency acoustic waves as a function of time (Torres, 2007). Ray tracing traditionally involves integrating a set of differential equations called the ray equations, which describe the ray's trajectory. The governing equations trace the path of a ray as it propagates away from the source by considering initial conditions.

The basis for ray theory is the acoustic wave equation, given in equation:

$$\nabla^2 p - \frac{1}{c^2}\frac{\partial^2 p}{\partial t^2} = 0, \tag{3}$$

where ∇ is the gradient operator, and c is the sound speed in the medium and may vary with the spatial coordinates (Urick, 1996). Separation of variables shown pressure depends on the three-dimensional position vector $\mathbf{x} = (x, y, z)$ and time t:

$$p = P(\mathbf{x}) \cdot T(t), \tag{4}$$

substituting this form into Eq. (3) and taking the separation constant to be k^2 obtain (Riley *et al.*, 1998):

$$\nabla^2 p - k^2 P = 0, \qquad \frac{\mathrm{d}^2 T}{\mathrm{d}t^2} + k^2 c^2 T = 0. \tag{5}$$

The first equation in Eq. (5) is the time-independent version of the acoustic wave equation, called the Helmholtz equation. Jensen *et al.* (2000) developed a solution of the Helmholtz equation of the form:

$$p(\mathbf{x}) = e^{i\omega\tau(\mathbf{x})} \sum_{j=0}^{\infty} \frac{A_j(\mathbf{x})}{(i\omega)^j}, \tag{6}$$

where $\tau(\mathbf{x})$ is the time, it takes for the sound to reach location $\mathbf{x}$, and $A(\mathbf{x})$ is the amplitude of the signal at $\mathbf{x}$. Equation (6) is called the ray series.

Thus, the pressure field is obtained by dividing the energy of the point source among each of the ray tubes. Since a point source in a shallow water channel follows spherical spreading, the sound pressure amplitude of a ray tube diminishes with range s by the factor $1/s^2$. The ratio of the pressure at a point a distance s from the source, $p(s)$, to the intensity measured at 1 m from the source, p_0, defines the TL at that point. For convenience, the TL along each ray tube is usually given in decibels [dB] (Torres, 2007):

$$\mathrm{TL}(st) = -20 \log \frac{p(s)}{p_0}. \tag{7}$$

The total pressure at the receiver will depend on how the rays constructively and destructively interfere with each other. There are several methods to solve this equation, and each of them has specific properties, which are listed in Table 1.

Ray theory calculates the TL based on the ray plotting. It is suitable for most operational applications due to its high speed and low computational volume. It is very effective for analyzing the acoustic propagation from a high-frequency source in large environments where the sound speed varies with distance. Since the Persian Gulf is shallow water, this method has been used to calculate TL in high frequency.

BELLHOP is an efficient ray-tracing model designed to perform acoustic ray tracing for a given sound speed profile $c(z)$ or a given sound speed field $c(r, z)$ in ocean waveguides with flat bed or variable absorbing boundaries. Output options include ray coordinates, travel time, amplitude, eigenrays, acoustic pressure, or TL (either coherent, incoherent, or semi-coherent)

Table 1. Domains of applicability of underwater acoustic propagation models (Etter, 2013).

Model type	Applications							
	Shallow water				Deep water			
	Low frequency (<500 Hz)		High frequency (>500 Hz)		Low frequency (<500 Hz)		High frequency (>500 Hz)	
	RI	RD	RI	RD	RI	RD	RI	RD
Ray theory	○	○	◑	●	◑	◑	●	●
Normal mode	●	◑	●	◑	●	◑	◑	○
Multipath expansion	○	○	◑	○	◑	○	●	○
Fast field	●	○	●	○	●	○	◑	○
Parabolic equation	◑	●	○	○	◑	●	◑	◑

RI – range-independent environment;

RD – range-dependent environment;

● – modelling approach is both applicable (physically) and practical (computationally);

◑ – limitations in accuracy or in speed of execution;

○ – neither applicable or practical.

(Porter, Bucker, 1987). The input of BELLHOP is an environmental file (*.env) to carry out ray tracing and TL; the information are given in Table 2 that we choose to design *.env, where we show the parameters used for modelling the effect of the warm eddy on acoustic propagation. Etter (2013) gives a guideline for defining the frequency above which a ray acoustics model becomes suitable for use. In the following equation:

$$f > 10\frac{c}{H}, \tag{8}$$

where f is the frequency, H is the water depth, and c is the sound speed. With a BELLHOP simulation depth of 60 m, and using an average sound speed of 1500 m/s, the formula resolves to $f > 250$ Hz. A frequency of 2 kHz, which is around the frequency range of a mid-frequency sonar, was used for the study and is well above the 375 Hz threshold. The BELLHOP simulation runs were conducted using the "incoherent" beam option, which allows a smoothed transmission loss plot of the sound energy over range.

Table 2. Parameters used for acoustic modelling.

Parameter	Value
Source data	
Number of sources	1
Source depth	25 m, 50 m
Source frequency	2 kHz
Source angle	−5 to +5
Receiver data	
Receiver ranges	0–154 km
Number of receiver ranges	3001
Receiver depths	0–82 m
Number of receiver depths	135
Number of rays	1000
Box depths	60 m
Box ranges	154 km
Options	
Method of interpolation	'QVW'
Type of media	'V*'
Type of output options	'IB'

3. Results and discussion

The algorithm results are obtained for 25 2-meter layers from the surface to a depth of 50 m. Figure 3 shows the eddies detected by the algorithm from the velocity field in early spring. In total, the detected number of cyclone eddies and anticyclone eddies are 4308 and 2860 in the surface layer, and 617 and 329 in the lowest layer 50 m depth, respectively. These eddies

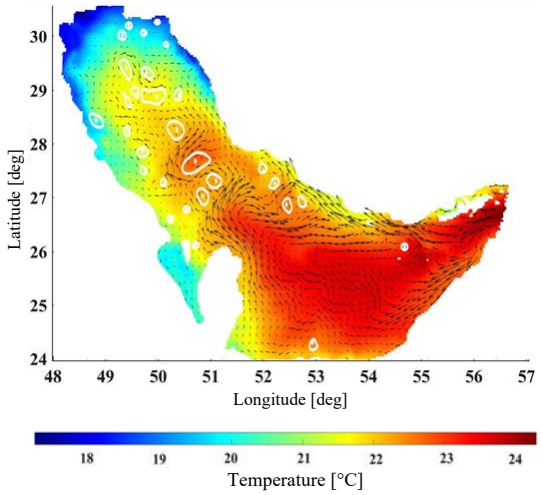

Fig. 3. Eddy field detected by the algorithm.

are positioned on the temperature distribution and have small diameters. In more detail, they form under the influence of local factors, such as topography or wind (Mahpeykar *et al.*, 2021).

Considering some uncertainties associated with the eddy detection scheme and sporadic noises in the numerical data, in the following analysis, we only count eddies which lifetimes are equal to or longer than three days (Dong *et al.*, 2012). Figure 4a shows the histogram of eddy sizes on the first day of their life that the radius of eddies can be approximately characterized by a normal distribution. Figure 4b illustrates that the lifespan of eddies varies from a few days to several weeks. The values of the positive and negative radius correspond to cyclone and anticyclone, respectively. As can be seen, most eddies have a radius of 5–10 km and are cyclonic types. This figure shows that sub-mesoscale eddies are the most abundant, and most of them are cyclonic. Histogram of eddy lifetimes also indicates that the occurrence of cyclonic eddies with a lifespan of more than three days is more than anticyclonic ones. The cause of the predominance of cyclonic eddies is the general circulation in the Persian Gulf, which is cyclonic. Therefore, the lifespan of the eddies in the Persian Gulf is affected by the thermohaline force. The inflow of the Oman Sea into the Persian Gulf is the main force that causes the development of cyclonic eddies.

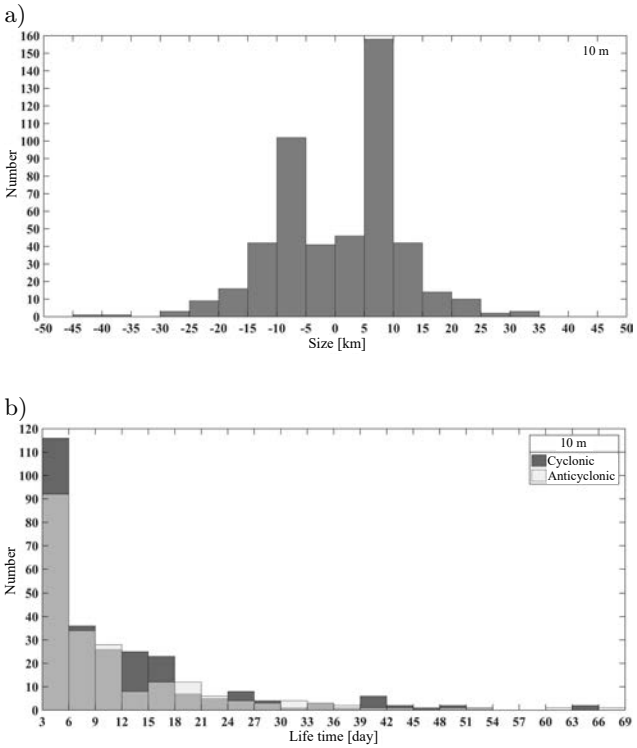

Fig. 4. Histograms of eddy initial sizes (a) and eddy lifetimes (b). On the left panel, the left and right sides of "0" on the x-axis denote the anticyclonic and cyclonic eddies, respectively.

One eddy with 29 days of lifespan was selected to investigate the acoustic propagation. The minimum and maximum calculated radii for the eddy are 4 and 48 km during its lifespan, respectively. This eddy is generally observed in 21 layers, and acoustic propagation around it was examined on the 26th day of its lifespan. Figure 5 shows the temperature and salinity profiles at the selected point. When the water column has an almost uniform temperature from the surface to the bed but it has significant differences in the transverse direction, an eddy is formed. Since an eddy is cyclonic, it makes sense to expect a cold core, and according to research carried out by Sun *et al.* (2019), an eddy causes divergence motion. In other words, in winter, the intense mixing can provide the initial energy to form an eddy due to the transverse temperature differences. So, the temperature difference causes the formation of an eddy, and the development of eddy has increased the temperature difference between the center of eddy and its surroundings, which is considered as positive feedback. It can be seen that the eddy is not well visible in the salinity profile due to the lack of salinity difference between the center of the eddy and its surroundings (Fig. 5).

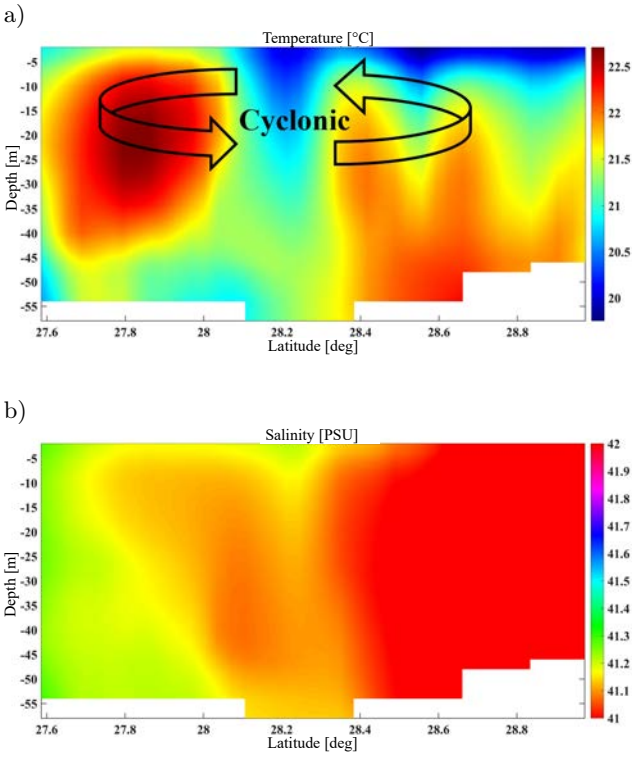

Fig. 5. Temperature (a) and salinity (b) profiles with eddy.

The distribution of sound speed is shown in Fig. 6 with/without the eddy to investigate the acoustic propagation. Because there is no strong stratification and vertical mixing in spring, sound speed was calculated for case "without eddy" in this season. Then, the acoustic propagation was examined under different scena-

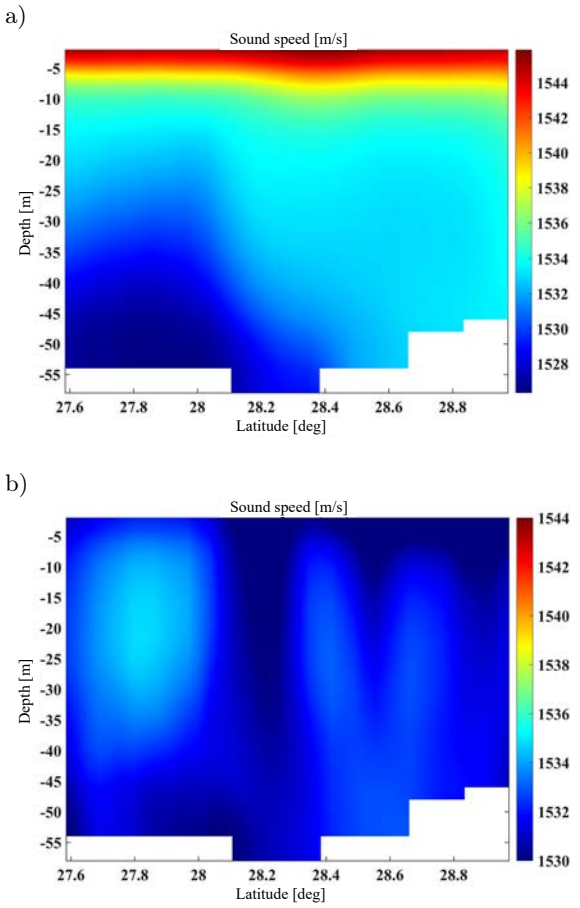

Fig. 6. Sound speed profile with (a) and without (b) eddy.

rios. The position of the eddy centre in the sound speed profile is quite clear under latitudes 28 to 28.4 degrees and a depth of 40 m. In the absence of eddy, the sound speed from the surface to the bed is reduced due to warming the surface layer in spring (Fig. 6b). In this case, the water column is stable, and the thermocline is on the formation threshold, nevertheless its effect on acoustic propagation is negligible because this condition becomes more severe in summer.

The pattern of TL when the source with a frequency of 2 kHz is located at 25 m depth with/without the eddy, taking into account the bed's topography, is shown in Fig. 7. Attenuation of acoustic pressure occurs in the presence of eddy radially around the source in these circumstances. The pressure reduction is less, and the acoustic rays travel longer distances without eddy than with eddy. The pressure is significantly reduced with eddy across the surface layer less than 5 m in depth. The most significant decrease of TL occurs along the travel distance after ~100 km with the eddy, and this reduction is the same from surface to bed.

Figure 8 shows the distribution of sound energy, in terms of TL, for the source deployed at 50 m depth and generating sound at 2 kHz with/without eddy. The TL in the presence of eddy is similar to the previous case,

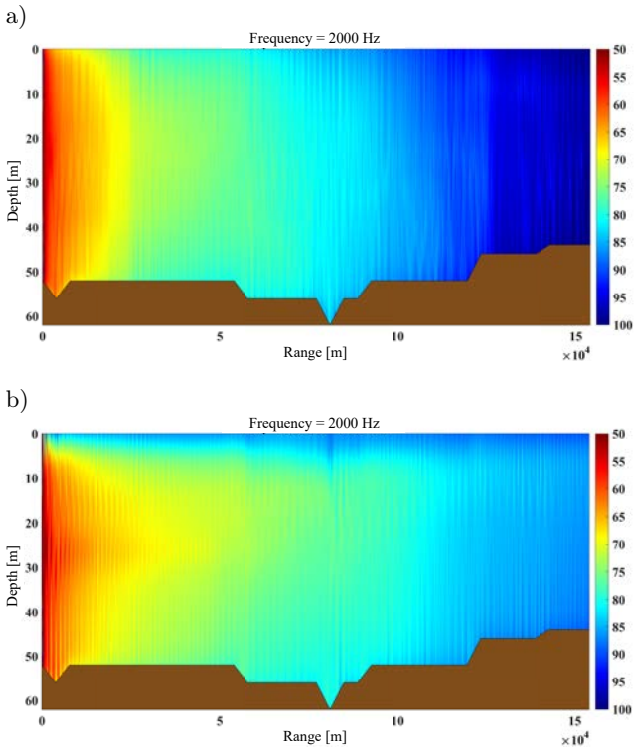

Fig. 7. Comparison of TLs [dB] for environments with (a) and without (b) eddy, with the source depth at 25 m.

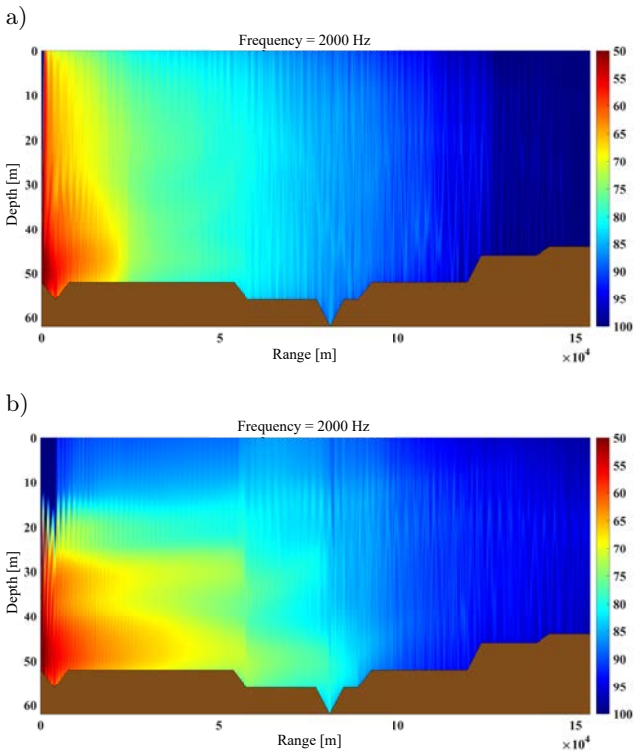

Fig. 8. Comparison of TLs [dB] for environments with (a) and without (b) eddy, with the source depth at 50 m.

but the pressure reduction is less near the source and seabed, and there is more reduction in the surface layer. The TL is lower in a quarter of the propagation

range close to the source without eddy, it increases suddenly outside of this range. This pattern is almost similar for both cases in the second half of the propagation range, but the TL is higher with eddy than without eddy, especially at the end of the range.

Figure 9 compares the TLs at two different depths of 25 m and 50 m. It is found that the TL at a depth of 25 m has a more considerable change than 50 m. The effect of the eddy is evident at a depth of 50 m at the beginning of the propagation range, but this difference increases step by step at a depth of 25 m. The most significant changes in temperature and salinity occur at the middle depths because the eddy radius is larger at there, so the TL is greater. Figure 9 shows the effect of the eddy at both depths that the TL is higher with eddy than without eddy, and as the distance from the source increases, the differences become greater. The decrease in TL is almost similar at the range close to the source and before the acoustic rays enter the eddy, but there is a sudden increase in the loss that is significant for the source at 50 m of depth (the range of 20 km from the source).

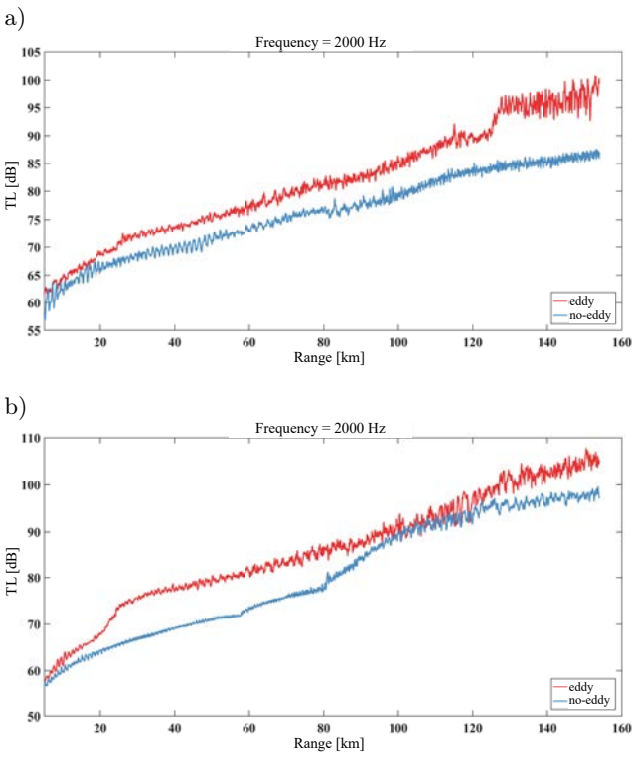

Fig. 9. TLs with/without eddy for the source and receivers at two depth of 25 m (a) and 50 m (b).

TL diagrams plotted for range-dependent with eddy (Fig. 10a), range-independent (Fig. 10b), and range-dependent without eddy (Fig. 10c), while the bed topography is omitted. A quantitative comparison could be made on how much eddy affects acoustic propagation in a model that does not account the environment. Source depth is 20 m, and its frequency

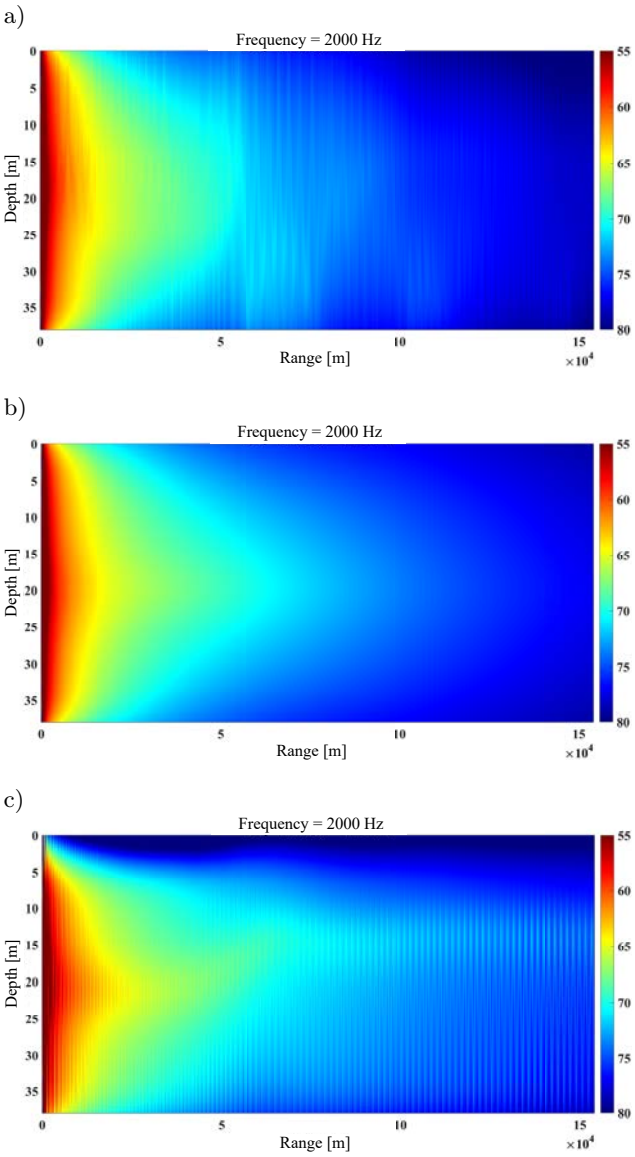

Fig. 10. Comparison of TLs among range-dependent with eddy (a), range-independent (b), and range-dependent without eddy (c).

is 2 kHz in all cases. TL is almost the same at all cases, especially in 30 km of the range close to source, fluctuations with a high amplitude are observed after a distance ~50 km in range-dependent with eddy. TL is seen uniformly and symmetrically across the propagation range in range-independent. Finally, for range-dependent without eddy (case c) the TL pattern is similar to case b, in the surface layer, less than 5 m, the sound pressure is significantly reduced, in agreement with the case where the topography was considered.

Now, we examine acoustic propagation in three dimensions with/without eddy at three different depths of 2 m, 25 m, and 50 m. Depth of 2 m is the depth at which acoustic equipment mounted on surface floats can operate. Obtained results presented by considering the bed's topography, as shown in Fig. 11. There

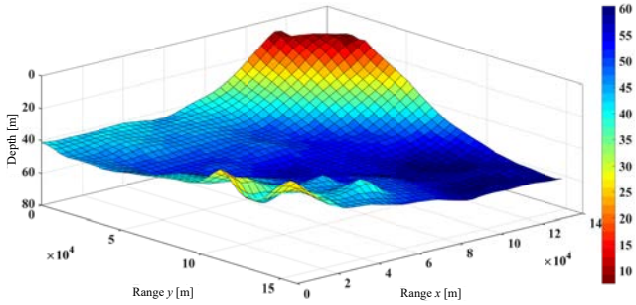

Fig. 11. Bed topography in the area of the desired eddy.

is a very steep slope on the coastal area that affects the acoustic propagation due to the location of the eddy centre in this position. Figure 12 shows the TL at three different depths with/without eddy. TL decreases uniformly as the range increases, but this reduction is non-uniform without eddy, and the acoustic rays travel more distance at specific angles. It is higher with eddy than without eddy at a radial distance of more than 30 km from the source. The TL changes seem reasonable around a central point because the geometry of the eddy is circular, it causes the temperature and salinity distributed radially around this point. The TL rate is slightly lower on the right side than the left ones with/without eddy; it can be attributed to the bed's topography because the deepest point exist in this region. There are little ups and downs on the left side, which have affected the TL, although the effect is negligible.

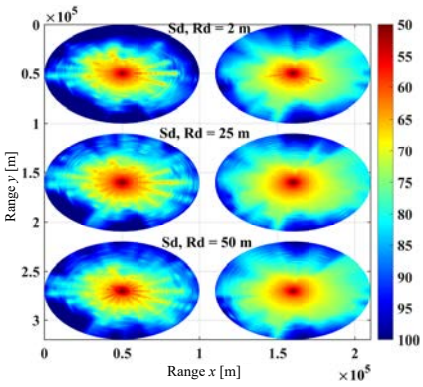

Fig. 12. Radial graph of TLs from an omnidirectional source deployed at different depth with (left side)/without (right side) eddy.

The TL changes are not very noticeable by increasing the source depth with eddy, and the rate of radial TL changes is similar for source and receivers at any depth. Change in the source and receivers depth has caused a change in the TL, and by moving away from the source, this difference has become significant, especially in 2 m. When the source was outside the eddy range with the acoustic ray passing through the eddy, as depth and distance increased, the TL increased in two-dimensional results. This is not seen in all directions in three-dimensional results, but in some angles and radius up to 50 km, the TL is less than other regions.

Because eddies affect the structure of temperature and salinity, they change the pattern and mode of acoustic propagation, and therefore the behaviour of acoustic varies from place to place. Acoustic propagation and TL in summer are very different from winter due to the occurrence of eddies because the stratified structure is dominant in this season. If the water column is stable, i.e. the warm surface water, the eddy does not play an influential role in water mass during acoustic propagation. Then, acoustic rays are directed towards the bottom, showing good agreement with previous studies (e.g. Lindar, Gawarkiewicz, 2006; Lam *et al.*, 2009).

The trend of change in TL is almost uniform along the propagation range in the cold eddy. This can be attributed to the symmetrical structure of the eddy due to the temperature and salinity distribution around the eddy centre. In other words, as the temperature decreases by approaching the eddy centre, it increases by moving away from the eddy centre. Therefore, there is no net difference during the whole propagation range. In general, the changes in TL relative to the propagation range have an exponential pattern, and this pattern has increased ~1 dB by reaching the eddy, it follows the original pattern after the eddy centre.

Studies on three-dimensional simulation of acoustic propagation around eddy have not been performed in shallow water. The role of forces in the stability and mixing of the water column is very important in acoustic propagation. The depth of the thermocline and its strength are determined directly by the surface heat flux, causing the vertical temperature gradient to change rapidly. This is accompanied by the stability of the water column, which also affects the structure of eddies. Furthermore, when the source is located near the bed, the bed topography features are important. Zarepoor *et al.* (2015) showed that the presence of the thermocline layer has remarkable effects on TL, increasing the gradient in the thermocline layer will raise TL.

4. Conclusions

The study of eddies using intelligent methods is very beneficial because the number of eddies and their spatial and temporal distribution is vast in the ocean and sea. Vector geometry algorithm, which operates based on the rotation of velocity vector, can detect eddies with high accuracy among the available methods. This algorithm is created to use in two dimensions typically, and its inputs are horizontal velocity components. In the present study, algorithm was developed to find eddies in three dimension, from the surface to 50 m of depth. The obtained eddies identified from the

numerical model outputs. Algorithm inputs are horizontal velocity components at a different layers.

This study showed a clear effect of eddies on acoustic propagation. Acoustic propagation in dynamic shallow waters is extremely complicated due to the high variability of oceanic processes (Katsnelson *et al.*, 2012). In the present research, the effect of the cold on acoustic propagation eddy was investigated. It was observed that the vertical structure of water is mixed, and the temperature and salinity in the Persian Gulf show slight changes from the surface to the bed. In these circumstances, the formation of an eddy causes the horizontal temperature gradient to be visible, so its presence can affect the sound speed in the environment. The salinity and temperature change around the eddy centre in the horizontal direction is such that those increase/decrease as it approaches the eddy centre, and this process is reversed as it moves away from the eddy center. The minimum or maximum values of temperature and salinity occur in the eddy center. Acoustic propagation has a lot to do with the physical properties of the marine environment, many studies have been done so far to investigate acoustic behaviour under the influence of different structures. In this study, the effect of eddy on acoustic propagation pattern was investigated in the Persian Gulf (as shallow water) for the first time. The results showed that the presence of eddy increases the TL compared to the one without eddy.

References

1. Chaigneau A., Gizolme A., Grados C. (2008), Mesoscale eddies off Peru in altimeter records: identification algorithms and eddy spatio-temporal patterns, *Progress Oceanography*, **79**(2–4): 106–119, doi: 10.1016/j.pocean.2008.10.013.
2. Chang Y.-L., Miyazawa Y., Béguer-Pon M. (2017), The dynamical impact of mesoscale eddies on migration of Japanese eel larvae, *PLoS ONE*, **12**(3): e0172501, doi: 10.1371/journal.pone.0172501.
3. Chang Y.-L., Miyazawa Y., Guo X. (2015), Effects of the STCC eddies on the Kuroshio based on the 20-year JCOPE2 reanalysis results, *Progress Oceanography*, **135**: 64–76, doi: 10.1016/j.pocean.2015.04.006.
4. Chelton D.B., Schlax M.G., Samelson R.M. (2011), Global observations of nonlinear mesoscale eddies, *Progress Oceanography*, **91**(2): 167–216, doi: 10.1016/j.pocean.2011.01.002.
5. Chen C., Gao Y., Yan F., Jin T., Zhou Z. (2019), Delving into the two-dimensional structure of a cold eddy east of Taiwan and its impact on acoustic propagation, *Acoustics Australia*, **47**: 185–193, doi: 10.1007/s40857-019-00160-7.
6. Dong C. *et al.* (2012), Three dimensional oceanic eddy analysis in the Southern California Bight from a numerical product, *Journal of Geophysical Research Oceans*, **117**: 1–17, doi: 10.1029/2011JC007354.
7. Etter P.C. (2013), *Underwater Acoustic Modeling and Simulation*, 4th ed., CRC Press.
8. Heathershaw A.D., Stretch C.E., Maskell S.J. (1991), Coupled ocean acoustic model studies of sound propagation through a front, *The Journal of the Acoustical Society of America*, **89**(1): 145–155, doi: 10.1121/1.400520.
9. Jensen F.B., Kuperman W.A., Porter M.B., Schmidt H. (2000), *Computational Ocean Acoustics*, Springer-Verlag New York Inc.
10. Katsnelson B., Petnikov V., Lynch J. (2012), *Fundamentals of Shallow Water Acoustics*, Springer.
11. Kochańska I., Schmidt J.H., Marszal J. (2020), Shallow water experiment of OFDM underwater acoustic communications, *Archives of Acoustics*, **45**(1): 11–18, doi: 10.24425/aoa.2019.129737.
12. Lam F.-P.A. *et al.* (2009), At-sea real-time coupled four-dimensional oceanographic and acoustic forecasts during Battlespace Preparation 2007, *Journal of Marine Systems*, **78**: 306–320, doi: 10.1016/j.jmarsys.2009.01.029.
13. Lermusiaux P.F.J., Xu J., Chen C.-F., Jan S., Chiu L.Y., Yang Y.-J. (2010), Coupled ocean–acoustic prediction of transmission loss in a continental shelfbreak region: predictive skill, uncertainty quantification, and dynamical sensitivities, *IEEE Journal of Oceanic Engineering*, **35**(4): 895–916, doi: 10.1109/JOE.2010.2068611.
14. Li J., Ren Z., Liu C., Fan H. (2012), Modeling of ocean mesoscale eddy and its application in the underwater acoustic propagation, *Marine Science Bulletin*, **14**(1): 1–15, http://hdl.handle.net/1834/14814.
15. Liang Z., Chunxia M., Haitao X. (2014), Comparison of sound propagation characteristic between deep and shallow water, *Applied Mechanics and Materials,* **577**: 1198–1201, doi: 10.4028/www.scientific.net/AMM.577.1198.
16. Linder C.A., Gawarkiewicz G.G. (2006), Oceanographic and sound speed fields for the ESME workbench, *IEEE Journal of Oceanic Engineering*, **31**(1): 22–32, doi: 10.1109/JOE.2006.872206.
17. Lynch J.F. *et al.* (2003), Spatial and temporal variations in acoustic propagation characteristics at the New England shelfbreak front, *IEEE Journal of Oceanic Engineering*, **28**(1): 129–150, doi: 10.1109/JOE.2003.808833.
18. Lysanov Y.P., Plotkin A.M., Shapiro G.I. (1989), The effect of intrathermocline lenses on acoustic fields in the ocean, *Izvestiya Akademii Nauk SSSR Fizika Atmosfery i Okeana*, **25**(12): 1272–1280, http://hdl.handle.net/10026.1/9752.
19. Mackenzie K.V., (1981), Nine-term equation for acoustic speed in the oceans, *The Journal of the Acous-*

tical Society of America, **70**: 807–812, doi: 10.1121/1.386920.

20. Mahpeykar O., Ashtari Larki A., Akbarinasab M. (2021), Numerical modelling and automatic detection of submesoscale eddies in Persian Gulf using a vector geometry algorithm, *Journal of the Earth and Space Physics*, **47**(1): 109–125, doi: 10.22059/JESPHYS.2021.307109.1007237.
21. Nencioli F., Dong C., Dickey T., Washburn L., McWillams J.C. (2010), A vector geometry–based eddy detection algorithm and its application to a high-resolution numerical model product and high-frequency radar surface velocities in the Southern California Bight, *Journal of Atmospheric and Oceanic Technology*, **27**: 564–579, doi: 10.1175/2009JTECHO725.1.
22. Peng Z., Fan J., Wang B. (2018), Analysis and modelling on radiated noise of a typical fishing boat measured in shallow water inspired by AQUO project's model, *Archives of Acoustics*, **43**(2): 263–273, doi: 10.24425/122374.
23. Peng Z., Zhou F., Fan J., Wang B., Wen H. (2021), Observation and modelling on the shipping noise in Shallow Waters with complex islands and reefs of the East China Sea, *Archives of Acoustics*, **46**(2): 301–311, doi: 10.24425/aoa.2021.136584.
24. Porter M.B., Bucker H.P. (1987), Gaussian beam tracing for computing ocean acoustic fields, *The Journal of the Acoustical Society of America*, **82**(4): 1349–1359, doi: 10.1121/1.395269.
25. Pous S., Lazure P., Carton X. (2015), A model of the general circulation in the Persian Gulf and in the Strait of Hormuz: Intraseasonal to interannual variability, *Continental Shelf Research*, **94**: 55–70, doi: 10.1016/j.csr.2014.12.008.
26. Reynolds R.M. (1993), Physical oceanography of the Gulf, Strait of Hormuz and the Gulf of Oman – Results from the Mt Mitchell expedition, *Marine Pollution Bulletin*, **27**: 35–59, doi: 10.1016/0025-326X(93)90007-7.
27. Riley K.F., Hobson M.P., Bence S.J. (1998), *Mathematical Methods for Physics and Engineering*, Cambridge University Press, Cambridge.
28. Sun W., Dong C., Tan W., He Y. (2019), Statistical characteristics of cyclonic warm-core eddies and anticyclonic cold-core eddies in the North Pacific based on remote sensing data, *Remote Sensing*, **11**(208): 1–22, doi: 10.3390/rs11020208.
29. Thoppil P.G., Hogan P.J. (2010), A modeling study of circulation and eddies in the Persian Gulf, *Journal of Physical Oceanography*, **40**: 2122–2134, doi: 10.1175/2010JPO4227.1.
30. Torres J.C. (2007), *Modeling of high-frequency acoustic propagation in shallow water*, Master's thesis, Department of Defense, Naval Postgraduate School.
31. Urick R.J. (1996), *Principles of Underwater Sound for Engineers,* 3rd ed., Peninsula Publishing.
32. Volkov D.L., Lee T., Fu L.-L. (2008), Eddy-induced meridional heat transport in the ocean, *Geophysical Research Letters*, **35**(20): 1–5, doi: 10.1029/2008GL035490.
33. Xiao Y., Li Z., Li J., Liu J., Sabra K.G. (2019), Influence of warm eddies on acoustic propagation in the Gulf of Mexico, *Chinese Physics B*, **28**(5): 1–11, doi: 10.1088/1674-1056/28/5/054301.
34. Xu J., Lermusiaux P.F., Haley Jr. P.J., Leslie W.G., Logutov O.G. (2008), Spatial and temporal variations in acoustic propagation during the PLUSNet'07 exercise in Dabob Bay, *Proceedings of Meetings on Acoustics*, **4**: 070001, doi: 10.1121/1.2988093.
35. Zarepoor V., Ezam M., Allahyaribeik S. (2015), Effect of thermocline formation on underwater acoustic waves propagation in Persian Gulf, *International Journal of Marine Science and Engineering*, **5**(1): 1–14, https://www.sid.ir/en/journal/ViewPaper.aspx?id=565610.
36. Zhang Z., Wang W., Qiu B. (2014), Oceanic mass transport by mesoscale eddies, *Science*, **345**(6194): 322–324, doi: 10.1126/science.1252418.